Advances in Applied Mathematics and Mechanics
Adv. Appl. Math. Mech., Vol. **xx**, No. x, pp. 1-26

DOI: 10.4208/aamm.OA-2023-0173
xxx 2025

The Spatial-Temporal Fourth-Order Conservative Characteristic Runge-Kutta Finite Difference Method for Convection-Dominated Diffusion Equation

Dan Qin[1], Kai Fu[1,*] and Dong Liang[2]

[1] *School of Mathematical Sciences, Ocean University of China, Qingdao, Shandong 266100, China*
[2] *Department of Mathematics and Statistics, York University, 4700 Keele Street, Toronto, M3J 1P3, Ontario, Canada*

Received 26 June 2023; Accepted (in revised version) 30 March 2024

Abstract. In this paper, we develop a new class of conservative characteristic finite difference methods for solving convection-dominated diffusion problems with fourth-order accuracy in both time and space. Specifically, the method of characteristics is utilized to handle the convection term, which allows for greater flexibility in the choice of time step sizes. To achieve high-order temporal accuracy, we propose characteristics-based optimal implicit strong stability preserving (SSP) Runge-Kutta methods implemented along the streamline. Furthermore, a conservative interpolation is employed to calculate values at the tracking points. By introducing diverse fourth-order approximation operators on the uniform Eulerian and irregular Lagrangian meshes, we can deal with the diffusion term with high accuracy while preserving the conservation property. The mass conservation for our proposed method is theoretically proved, and is verified through numerical experiments. Moreover, the numerical tests demonstrate that our scheme achieves temporal and spatial fourth-order accuracy and generates non-oscillatory solutions, even with large time step sizes.

AMS subject classifications: 65M25, 65N06

Key words: Convection-dominated diffusion equations, spatial-temporal fourth-order, mass conservation, characteristic method.

1 Introduction

Many physical phenomena can be modeled by partial differential equations, among which the convection-diffusion equation holds significant importance with a wide range of

*Corresponding author.
Emails: qd@stu.ouc.edu.cn (D. Qin), kfu@ouc.edu.cn (K. Fu), dliang@yorku.ca (D. Liang)

applications, such as fluid flowing, atmospheric environment simulation, groundwater modeling and financial computation [3, 12, 28]. In the realm of fluid dynamics, the intricate interplay between convection and diffusion plays a pivotal role in ascertaining the stability and dynamics of fluid systems [31, 32], thus convection-diffusion problems have been extensively studied over the years. Unfortunately, finding the exact solution to convection-diffusion equations is often impractical or impossible, leading to the development of reliable numerical schemes with high precision to solve the problem [12, 14, 16, 22, 23, 36, 38]. This research is crucial as it enables further exploration of physical phenomena and properties of systems governed by convection-diffusion equations.

In consideration of large computational regions and long period prediction, one of the key indicators of numerical methods is computational efficiency. When numerically solving convection-diffusion equations, particularly in cases where convection dominates diffusion, traditional schemes suffer from severe CFL restrictions and require fine time discretization with high computational costs [2, 5]. To address these issues, specific techniques have been developed to treat the convection term with care [9, 13, 16, 19, 27, 34]. The characteristics method is particularly attractive in that problems can be solved effectively along the streamline with high-order accuracy, resulting in significant computational savings. Over the years, many numerical schemes based on characteristics technique have been proposed to solve convection-diffusion equation [1, 4, 8–12, 14, 18, 23–26, 29, 35, 37, 39], which avoid the issues of non-physical oscillations and excessive numerical dissipation at steep fronts even with the coarse time step sizes [10]. In the realm of one-dimensional convection-diffusion problems, a modified method of characteristics was first proposed by Douglas and Russell in [9], which possesses first-order accuracy in time. Since then, temporal first-order characteristic methods have been further developed and applied to problems in high dimensions including aerosol transport and miscible displacement in porous media [4, 8, 18, 25, 26, 35]. However, these techniques can't guarantee mass conservation, which is a critical requirement for various mathematical modeling applications [15]. To overcome this limitation, Arbogast and Wheeler developed a characteristics-mixed finite element method conserving mass based on a space-time variational form of the convection-diffusion equation in [1]. Furthermore, temporal second-order conservative characteristic schemes have been proposed [29, 39] and further developed. [10] introduced a temporal second-order and spatial high-order scheme to deal with the aerosol convection-diffusion process. In the context of two-dimensional convection-diffusion problems, a spatial second-order conservative characteristic scheme was developed in [11], and later [12] achieved fourth-order spatial accuracy.

To enhance the accuracy of time discretization in computational simulations, numerous temporal high-order schemes have been devised. A notable category among these schemes is the strong stability preserving (SSP) temporal discretizations, which are first tailored to ensure the stability properties of the numerical solutions to hyperbolic problems [17]. These methods are known for their ability to preserve the strong stability properties of the spatial discretization coupled with the first-order Euler temporal discretiza-

tion. The SSP Runge-Kutta methods, which can be viewed as convex combinations of several forward Euler steps, have been employed with various spatial discretizations and proven useful in numerous applications, such as atmospheric transport [33], Maxwell's equations [30] and compressible flow [6]. Despite their usefulness, the application of SSP Runge-Kutta methods in combination with the characteristic technique poses challenges due to the involvement of tracing the Eulerian mesh.

We develop in this work spatial-temporal fourth-order conservative finite difference schemes for solving the convection-dominated diffusion problem. By combining the characteristics technique with high-order conservative interpolation [7, 12], it allows the use of large time step sizes without sacrificing the conservation property. In order to deal with the diffusion term with variable coefficients, we introduce different fourth-order approximation operators based on uniform Eulerian mesh and irregular Lagrangian mesh, which have fourth order accuracy in space and preserve the mass conservation. Moreover, the characteristics-based optimal implicit strong stability preserving Runge-Kutta methods are introduced and applied along the streamline to achieve temporal high-order accuracy. The mass conservation property for the proposed scheme has been rigorously proved. Numerical experiments demonstrate the temporal and spatial convergence orders of our proposed scheme. Furthermore, it is observed that our numerical method maintains mass conservation and effectively avoids numerical oscillations, even when using large time step sizes. This method offers significant practical applications in various fields where convection-dominated diffusion equations arise, such as in environmental modeling, fluid mechanics, and financial simulations.

The paper is organized as follows. In Section 2, we present the conservative characteristic spatial-temporal fourth-order finite difference method (CC-S4T4-FDM) for one-dimensional convection-dominated diffusion equations and prove its mass conservation property. In Section 3, we extend the constructed scheme and theoretical proof to the two-dimensional case. Numerical experiments for validating the effectiveness and accuracy of proposed scheme are presented in Section 4. Conclusion is given in Section 5.

2 One-dimensional case

We first consider the one-dimensional convection-diffusion problem in the domain $\Omega = [a,b]$,

$$\frac{\partial c}{\partial t} + u\frac{\partial c}{\partial x} - \frac{\partial}{\partial x}\left(K(x)\frac{\partial c}{\partial x}\right) = 0, \qquad (x,t) \in \Omega \times (0,T], \tag{2.1a}$$

$$c(x,0) = c_0(x), \qquad x \in \Omega, \tag{2.1b}$$

where $(0,T]$ is the time period, $u = u(t)$ is the velocity of the field and $K(x) \in C^1(\Omega)$ with $0 < K_{\min} \le K(x) \le K_{\max}$ is the diffusion coefficient. $c_0(x)$ is the initial condition and we apply the periodic boundary condition here.

Let $L\equiv b-a$ and divide $\Omega=[a,b]$ by the uniform partition

$$a=x_{\frac{1}{2}}<x_{\frac{3}{2}}<\cdots<x_{I+\frac{1}{2}}=b,$$

which satisfies $x_{i+\frac{1}{2}}=a+ih$ for $i=0,1,\cdots,I$ with $h\equiv L/I$. Then cells and cell centers are defined by

$$\Omega_i=[x_{i-\frac{1}{2}},x_{i+\frac{1}{2}}],\quad x_i=\frac{1}{2}(x_{i-\frac{1}{2}}+x_{i+\frac{1}{2}}),\quad i=1,2,\cdots,I.$$

Consider N_t as the time steps with $\Delta t=T/N_t$, then define $t^n=n\Delta t$.

For proposing the characteristic method, consider the variable x as a function of the variable t, i.e., $x=X(t)$. Then the characteristic line associated with a location x^* at t^* in the time interval $[t^n,t^{n+1}]$ satisfies the ordinary differential equation

$$\begin{cases}\dfrac{dX(t;t^*,x^*)}{dt}=u(X(t;t^*,x^*),t),\quad t\in[t^n,t^{n+1}],\\ X(t^*;t^*,x^*)=x^*.\end{cases}\tag{2.2}$$

Introducing the representation of the Lagrangian derivative of the unknown quantity c following the fluid, i.e., $d/dt=\partial/\partial t+u\partial/\partial x$, it follows that the problem (2.1a) can be rewritten in the form

$$\frac{dc}{dt}=\frac{\partial}{\partial x}\left(K\frac{\partial c}{\partial x}\right).\tag{2.3}$$

2.1 Spatial semi-discretization

In order to handle the diffusion term of (2.3) on the uniform Eulerian mesh with high-order accuracy, we introduce the finite difference approximation operator $\mathcal{P}$ as in [12, 21], which has fourth-order spatial accuracy for the differential operator $\frac{\partial}{\partial x}(K\frac{\partial\cdot}{\partial x})$ under the variable coefficient case. Let K_i and $C_i=C_i(t)$ represent $K(x_i)$ and the numerical approximation for $c(x_i,t)$, respectively, then the operator $\mathcal{P}$ can be defined as

$$\mathcal{P}(C)_i=\frac{H_{i+\frac{1}{2}}(C)-H_{i-\frac{1}{2}}(C)}{h}\tag{2.4}$$

with $H(\cdot)$ being the high-order discretized flux defined by

$$H_{i+\frac{1}{2}}(C)=\frac{1}{h}\sum_{l=-1}^{2}\sum_{m=-1}^{2}M_{l,m}K_{i+l}C_{i+m},\tag{2.5}$$

where $M=\{M_{l,m}\}$ is given by

$$M=\begin{bmatrix} \frac{1}{8} & -\frac{1}{6} & \frac{1}{24} & 0 \\ -\frac{1}{6} & -\frac{3}{8} & \frac{2}{3} & -\frac{1}{8} \\ \frac{1}{8} & -\frac{2}{3} & \frac{3}{8} & \frac{1}{6} \\ 0 & -\frac{1}{24} & \frac{1}{6} & -\frac{1}{8} \end{bmatrix}. \tag{2.6}$$

The size of tracking cell remains unchanged with the velocity being independent of spatial variable, thus the operator $\mathcal{P}$ for the diffusion term defined on the uniform Eulerian mesh can also be applied on the tracking mesh. Then we can achieve the spatial fourth-order semi-discretization scheme of (2.3) with the above operator $\mathcal{P}$, which is written as

$$\frac{dC_i}{dt}=\mathcal{P}(C)_i. \tag{2.7}$$

2.2 Characteristic SSP scheme

Now we construct the full-discretization scheme in the time interval $[t^n,t^{n+1}]$ to calculate the numerical solution of the one-dimensional convection-diffusion problem (2.1a). In order to calculate C_i^{n+1} as an approximation of $c(x_i,t^{n+1})$ using the characteristic method, we need to know the value at the tracking point of the previous time level.

For the need of mass conservation, we now regard the numerical solution C_i as the average value of the corresponding interval Ω_i for every time level. Trace the interval Ω_i along characteristics from t^{n+1} to t^n and denote the tracking interval by

$$\bar{\Omega}_i^{(0)}=\left[X(t^n;t^{n+1},x_{i-\frac{1}{2}}),\ X(t^n;t^{n+1},x_{i+\frac{1}{2}})\right]\equiv[\bar{x}_{i-\frac{1}{2}},\bar{x}_{i+\frac{1}{2}}],$$

which can be identified by solving the problem (2.2) under the conditions of $X(t^{n+1})=x_{i-\frac{1}{2}}$ and $X(t^{n+1})=x_{i+\frac{1}{2}}$ with the fourth-order Runge-Kutta method. Next we calculate the approximation for the integral of $c(x,t^n)$ over the tracking interval $\bar{\Omega}_i^{(0)}$.

As in [10], we apply the conservative piecewise parabolic method [7, 12] to construct a particular parabolic interpolation polynomial $[\mathcal{R}C^n](x)$ at $t=t^n$. Define

$$\begin{aligned}[\mathcal{R}C^n]_p(x)=&\langle C^n\rangle_{p-\frac{1}{2}}+\frac{x-x_{p-\frac{1}{2}}}{h}\Bigg(\langle C^n\rangle_{p+\frac{1}{2}}-\langle C^n\rangle_{p-\frac{1}{2}}\\&+6\left(C_p^n-\frac{1}{2}(\langle C^n\rangle_{p+\frac{1}{2}}+\langle C^n\rangle_{p-\frac{1}{2}})\right)\frac{x_{p+\frac{1}{2}}-x}{h}\Bigg)\end{aligned} \tag{2.8}$$

on every interval Ω_p, where $\langle C^n\rangle_{p+\frac{1}{2}}$ is calculated for the fourth-order accuracy in space as below:

$$\langle C^n\rangle_{p+\frac{1}{2}}=\frac{7}{12}(C_p^n+C_{p+1}^n)-\frac{1}{12}(C_{p+2}^n+C_{p-1}^n). \tag{2.9}$$

Note that the size of tracking interval $\bar{\Omega}_i^{(0)}$ is still h, which may coincide with some Eulerian cell or take up two subdivision intervals for the one-dimensional case. Thus $\int_{\bar{\Omega}_i^{(0)}}c(x,t^n)dx$ can be evaluated as

$$\begin{aligned}\int_{\bar{\Omega}_i^{(0)}}c(x,t^n)dx&\approx\int_{\bar{x}_{i-\frac{1}{2}}}^{\bar{x}_{i+\frac{1}{2}}}[\mathcal{R}C^n](x)dx\\&=\int_{\bar{x}_{i-\frac{1}{2}}}^{x_{l+\frac{1}{2}}}[\mathcal{R}C^n]_l(x)dx+\int_{x_{l+\frac{1}{2}}}^{\bar{x}_{i+\frac{1}{2}}}[\mathcal{R}C^n]_{l+1}(x)dx\\&\equiv\mathcal{R}_{\bar{\Omega}_i^{(0)}}(C^n),\end{aligned} \tag{2.10}$$

where l is the cell index associated with the segment in which $\bar{x}_{i-\frac{1}{2}}$ lies, i.e., $\bar{x}_{i-\frac{1}{2}}\in\Omega_l$. Then we let the mean value

$$\frac{1}{h}\mathcal{R}_{\bar{\Omega}_i^{(0)}}(C^n)\equiv\bar{C}_i^{(0)}$$

represent the approximation for $c(x,t)$ at the tracking point $X(t^n;t^{n+1},x_i)\equiv\bar{x}_i$ without breaking the property of mass conservation.

Now we propose the conservative characteristic spatial-temporal fourth-order finite difference method (CC-S4T4-FDM) combined with the optimal three-stage fourth-order implicit SSP Runge-Kutta method for solving the one-dimensional convection-diffusion problem (2.1a)-(2.1b)

$$\bar{C}_i^{(0)}=\frac{1}{h}\mathcal{R}_{\bar{\Omega}_i^{(0)}}(C^n), \tag{2.11a}$$

$$\bar{C}_i^{(1)}=v_1\bar{C}_i^{(0)}+\Delta t\beta_{11}\mathcal{P}(\bar{C}^{(1)})_i, \tag{2.11b}$$

$$\bar{C}_i^{(2)}=v_2\bar{C}_i^{(0)}+\alpha_{21}\bar{C}_i^{(1)}+\Delta t\beta_{21}\mathcal{P}(\bar{C}^{(1)})_i+\Delta t\beta_{22}\mathcal{P}(\bar{C}^{(2)})_i, \tag{2.11c}$$

$$\bar{C}_i^{(3)}=v_3\bar{C}_i^{(0)}+\alpha_{32}\bar{C}_i^{(2)}+\Delta t\beta_{32}\mathcal{P}(\bar{C}^{(2)})_i+\Delta t\beta_{33}\mathcal{P}(\bar{C}^{(3)})_i, \tag{2.11d}$$

$$\begin{aligned}C_i^{n+1}=&v_4\bar{C}_i^{(0)}+\alpha_{41}\bar{C}_i^{(1)}+\alpha_{42}\bar{C}_i^{(2)}+\alpha_{43}\bar{C}_i^{(3)}+\Delta t\beta_{41}\mathcal{P}(\bar{C}^{(1)})_i\\&+\Delta t\beta_{42}\mathcal{P}(\bar{C}^{(2)})_i+\Delta t\beta_{43}\mathcal{P}(\bar{C}^{(3)})_i.\end{aligned} \tag{2.11e}$$

The coefficients v_p, $\alpha_{p,q}$ and $\beta_{p,q}$ above are consistent with the coefficients of the optimal three-stage fourth-order implicit SSP Runge-Kutta method in [17], which satisfy the consistency requirements

$$v_p+\sum_q\alpha_{p,q}=1,\quad p=1,2,3,4. \tag{2.12}$$

For a clear description, we define

$$t^{(0)}=0,\quad t^{(1)}=\beta_{11}\Delta t,\quad t^{(2)}=(\alpha_{21}\beta_{11}+\beta_{21}+\beta_{22})\Delta t, \tag{2.13a}$$

$$t^{(3)}=[\alpha_{32}(\alpha_{21}\beta_{11}+\beta_{21}+\beta_{22})+\beta_{32}+\beta_{33}]\Delta t,\quad t^{(4)}=\Delta t, \tag{2.13b}$$

and represent the tracking interval $\bar{\Omega}_i^{(k)}$ as

$$\bar{\Omega}_i^{(k)}=\left[X(t^n+t^{(k)};t^{n+1},x_{i-\frac{1}{2}}),\ X(t^n+t^{(k)};t^{n+1},x_{i+\frac{1}{2}})\right],\quad k=0,1,2,3, \tag{2.14}$$

which are specifically shown in Fig. 1. Then $\bar{C}_i^{(0)}$, $\bar{C}_i^{(1)}$, $\bar{C}_i^{(2)}$ and $\bar{C}_i^{(3)}$ in the intermediate process of the proposed method (2.11a)-(2.11e) are obtained by computing the approximation for the average of solution on $\bar{\Omega}_i^{(0)}$, $\bar{\Omega}_i^{(1)}$, $\bar{\Omega}_i^{(2)}$ and $\bar{\Omega}_i^{(3)}$, respectively.

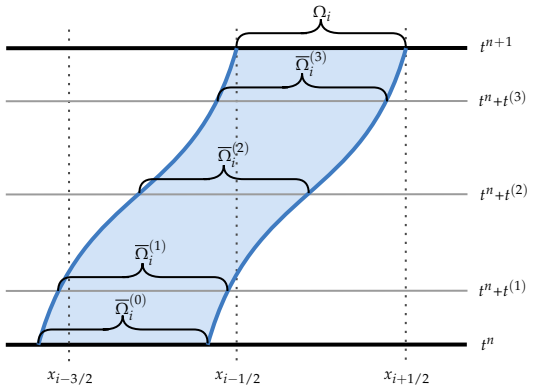

Figure 1: The schematic diagram for the characteristic tracking of Ω_i.

Remark 2.1. There are many other strong stability preserving Runge–Kutta methods which are different convex combinations of several formal forward Euler steps [17]. These methods can be similarly applied to construct other temporal high-order conservative numerical schemes without breaking the mass conservation property of the solution. The above results can be easily extended to multiple-dimensional cases.

2.3 Mass conservation

Theorem 2.1. *The proposed scheme* (2.11a)-(2.11e) *for solving the one-dimensional convection-diffusion problem* (2.1a) *with the periodic boundary condition is globally mass conservative.*

Proof. Multiplying (2.11b) by h and summing for i from 1 to I, it follows that

$$\sum_{i=1}^{I}h\bar{C}_i^{(1)}=v_1\sum_{i=1}^{I}h\bar{C}_i^{(0)}+\Delta t\beta_{11}\sum_{i=1}^{I}h\mathcal{P}(\bar{C}^{(1)})_i. \tag{2.15}$$

According to the definition of $\bar{C}_i^{(0)}$ and (2.10), it can be known that

$$\sum_{i=1}^{I} h\bar{C}_i^{(0)} = \sum_{i=1}^{I} \mathcal{R}_{\bar{\Omega}_i^{(0)}}(C^n) = \sum_{i=1}^{I} hC_i^n \tag{2.16}$$

under the periodic boundary condition. It also yields

$$\begin{aligned}\sum_{i=1}^{I} h\mathcal{P}(\bar{C}^{(1)})_i &= \sum_{i=1}^{I} \left(H_{i+\frac{1}{2}}(\bar{C}^{(1)}) - H_{i-\frac{1}{2}}(\bar{C}^{(1)}) \right) \\ &= H_{I+\frac{1}{2}}(\bar{C}^{(1)}) - H_{\frac{1}{2}}(\bar{C}^{(1)}) = 0.\end{aligned} \tag{2.17}$$

Note that $v_1 = 1$ according to (2.12), then we know

$$\sum_{i=1}^{I} h\bar{C}_i^{(1)} = \sum_{i=1}^{I} hC_i^n. \tag{2.18}$$

Similarly, we multiply (2.11c) by h and sum for i from 1 to I. According to (2.16) and (2.18), we have

$$\sum_{i=1}^{I} h\bar{C}_i^{(2)} = (v_2+\alpha_{21}) \sum_{i=1}^{I} hC_i^n + \Delta t\beta_{21} \sum_{i=1}^{I} h\mathcal{P}(\bar{C}^{(1)})_i + \Delta t\beta_{22} \sum_{i=1}^{I} h\mathcal{P}(\bar{C}^{(2)})_i.$$

Considering the periodic boundary condition and (2.12), we can know that

$$\begin{aligned}\sum_{i=1}^{I} h\mathcal{P}(\bar{C}^{(2)})_i &= \sum_{i=1}^{I} \left(H_{i+\frac{1}{2}}(\bar{C}^{(2)}) - H_{i-\frac{1}{2}}(\bar{C}^{(2)}) \right) \\ &= H_{I+\frac{1}{2}}(\bar{C}^{(2)}) - H_{\frac{1}{2}}(\bar{C}^{(2)}) = 0, \\ v_2+\alpha_{21} &= 1,\end{aligned}$$

then it yields

$$\sum_{i=1}^{I} h\bar{C}_i^{(2)} = \sum_{i=1}^{I} hC_i^n. \tag{2.19}$$

Based on the similar analysis, we have

$$\sum_{i=1}^{I} hC_i^{n+1} = \sum_{i=1}^{I} hC_i^n. \tag{2.20}$$

Thus, we complete the proof. □

3 Two-dimensional case

Now we introduce the spatial-temporal fourth-order conservative characteristic scheme for the two-dimensional convection-diffusion problem in the domain $\Omega=[a_x,b_x]\times[a_y,b_y]$,

$$\frac{\partial c}{\partial t}+\boldsymbol{u}\cdot\nabla c(x,y,t)-\nabla\cdot(K\nabla c(x,y,t))=0, \qquad (x,y,t)\in\Omega\times(0,T], \tag{3.1a}$$

$$(K\nabla c)\cdot\boldsymbol{n}=0, \qquad (x,y,t)\in\partial\Omega\times(0,T], \tag{3.1b}$$

$$c(x,y,0)=c_0(x,y), \qquad (x,y)\in\Omega, \tag{3.1c}$$

where c is the quantity to be calculated at spatial location $\boldsymbol{x}=(x,y)$ and time t. $\boldsymbol{u}=(u^x,u^y)$ is the convection coefficient, which satisfies $\nabla\cdot\boldsymbol{u}=0$. $K=\mathrm{diag}(K^x(x,y),K^y(x,y))$ is a diagonal diffusion coefficient matrix with $K^x,K^y\in C^1(\Omega)$, and there are two positive constants $K_{\min}$ and $K_{\max}$, such that $0<K_{\min}\le K^x,\ K^y\le K_{\max}$. $\partial\Omega$ denotes the boundary of Ω and $\boldsymbol{n}$ is the unit outer normal to the boundary $\partial\Omega$. T represents the final time. We assume sufficient smoothness of all the variables along spatial direction.

Let $L_x\equiv b_x-a_x$, $L_y\equiv b_y-a_y$. Consider the uniform partition of the domain $\Omega=[a_x,b_x]\times[a_y,b_y]$ as follows:

$$\begin{aligned} a_x&=x_{\frac12}<x_{\frac32}<\cdots<x_{I+\frac12}=b_x,\\ a_y&=y_{\frac12}<y_{\frac32}<\cdots<y_{J+\frac12}=b_y, \end{aligned}$$

which satisfies $x_{i+\frac12}=a_x+ih_x$ and $y_{j+\frac12}=a_y+jh_y$ with $h_x\equiv L_x/I$ and $h_y\equiv L_y/J$. Then, for $i=1,2,\cdots,I$ and $j=1,2,\cdots,J$, cells and cell centers are defined by

$$\begin{aligned} &\Omega_{i,j}=[x_{i-\frac12},x_{i+\frac12}]\times[y_{j-\frac12},y_{j+\frac12}],\\ &x_i=\frac12(x_{i-\frac12}+x_{i+\frac12}),\quad y_j=\frac12(y_{j-\frac12}+y_{j+\frac12}). \end{aligned}$$

Let N_t represent the time steps with $\Delta t=T/N_t$, and set $t^n=n\Delta t$. Consider the variable $\boldsymbol{x}$ as a function of the variable t, i.e., $\boldsymbol{x}=\boldsymbol{X}(t)$, then the characteristic line associated with a location $\boldsymbol{x}^*$ at t^* in the time interval $[t^n,t^{n+1}]$ satisfies the ordinary differential equation

$$\begin{cases} \dfrac{d\boldsymbol{X}(t\,;t^*,\boldsymbol{x}^*)}{dt}=\boldsymbol{u}(\boldsymbol{X}(t\,;t^*,\boldsymbol{x}^*),t), \quad t\in[t^n,t^{n+1}],\\ \boldsymbol{X}(t^*;t^*,\boldsymbol{x}^*)=\boldsymbol{x}^*. \end{cases} \tag{3.2}$$

Now we use the representation of the Lagrangian derivative of the unknown quantity c following the fluid, i.e., $d/dt=\partial/\partial t+\boldsymbol{u}\cdot\nabla$, then Eq. (3.1a) can be rewritten in the form

$$\frac{dc}{dt}=\frac{\partial}{\partial x}\left(K^x\frac{\partial c}{\partial x}\right)+\frac{\partial}{\partial y}\left(K^y\frac{\partial c}{\partial y}\right). \tag{3.3}$$

3.1 Spatial semi-discretization

Now we introduce the finite difference approximation operator $\mathcal{Q}$ for the diffusion term $\frac{\partial}{\partial x}(K^x\frac{\partial \cdot}{\partial x})+\frac{\partial}{\partial y}(K^y\frac{\partial \cdot}{\partial y})$ of (3.3) on the uniform Eulerian mesh, which is spatial fourth-order accuracy [12]. Let $\boldsymbol{x}_{i,j}=(x_i,y_j)$ and denote $K^x(\boldsymbol{x}_{i,j})$, $K^y(\boldsymbol{x}_{i,j})$ and the numerical approximation for $c(\boldsymbol{x}_{i,j},t)$ as $K^x_{i,j}$, $K^y_{i,j}$ and $C_{i,j}=C_{i,j}(t)$, respectively. Next we define the approximation operator $\mathcal{Q}$ as

$$\mathcal{Q}(C)_{i,j}=\frac{\hat{H}_{i+\frac{1}{2},j}(C)-\hat{H}_{i-\frac{1}{2},j}(C)}{h_x}+\frac{\hat{H}_{i,j+\frac{1}{2}}(C)-\hat{H}_{i,j-\frac{1}{2}}(C)}{h_y}, \tag{3.4}$$

with $\hat{H}(\cdot)$ being the continuous flux defined by

$$\hat{H}_{i+\frac{1}{2},j}(C)=\frac{1}{h_x}\sum_{l=-1}^{2}\sum_{m=-1}^{2}M_{l,m}K^x_{i+l,j}C_{i+m,j}, \tag{3.5}$$

$$\hat{H}_{i,j+\frac{1}{2}}(C)=\frac{1}{h_y}\sum_{l=-1}^{2}\sum_{m=-1}^{2}M_{l,m}K^y_{i,j+l}C_{i,j+m}, \tag{3.6}$$

where $M=\{M_{l,m}\}$ is given by (2.6) as the one-dimensional case. Noting that "ghost cells" are needed for implementing calculation at the boundary, thus we define $C_{0,j}$, $C_{-1,j}$, $C_{I+1,j}$ and $C_{I+2,j}$ as in [12], meanwhile $C_{i,0}$, $C_{i,-1}$, $C_{i,J+1}$ and $C_{i,J+2}$ are computed similarly.

For keeping the mass conservation, we regard the numerical solution $C_{i,j}$ as the average value on the corresponding cell $\Omega_{i,j}$ for every time level. Because of using the characteristic technique, it is essential to know the value at the tracking point along the characteristics first.

For the Eulerian cell $\Omega_{i,j}$ at $t=t^{n+1}$, denote its tracking cell at $t=t^n$ by $\bar{\Omega}_{i,j}$ (Fig. 2), which is usually irregular and is identified by solving the problem (3.2). Then the integral of the solution over $\bar{\Omega}_{i,j}$ can be approximated with the one-dimensional conservative interpolation reconstruction technique define in (2.8)-(2.9) in two stages [10,12].

Stage 1. Conservative interpolation along the Eulerian x-direction for the areas between the Eulerian lines $y_{j-\frac{1}{2}}$ and $y_{j+\frac{1}{2}}$. Construct fourth-order accuracy conservative interpolation along the Eulerian x-direction based on $C^n_{p,j}$, $p=1,2,\cdots,I$. Then the mass, i.e., the integral of the constructed interpolation can be calculated over each intermediate cell $\hat{\Omega}_{i,j}$ (Fig. 2), the area bounded by $y_{j-\frac{1}{2}}$, $y_{j+\frac{1}{2}}$, $\mathcal{L}x_{i-\frac{1}{2}}$ and $\mathcal{L}x_{i+\frac{1}{2}}$.

Stage 2. Conservative interpolation along the Lagrangian y-direction for the area between the Lagrangian lines $\mathcal{L}x_{i-\frac{1}{2}}$ and $\mathcal{L}x_{i+\frac{1}{2}}$. Using the calculated masses over the intermediate cells, we perform a similar operation as in Stage 1. Denote the integral of the constructed piecewise parabolic interpolation polynomial over $\bar{\Omega}_{i,j}$ by $\mathcal{I}_{\bar{\Omega}_{i,j}}(C^n)$.

Then the value at the tracking point is approximated by

$$\frac{1}{h_xh_y}\mathcal{I}_{\bar{\Omega}_{i,j}}(C^n)\equiv\bar{C}^n_{i,j}$$

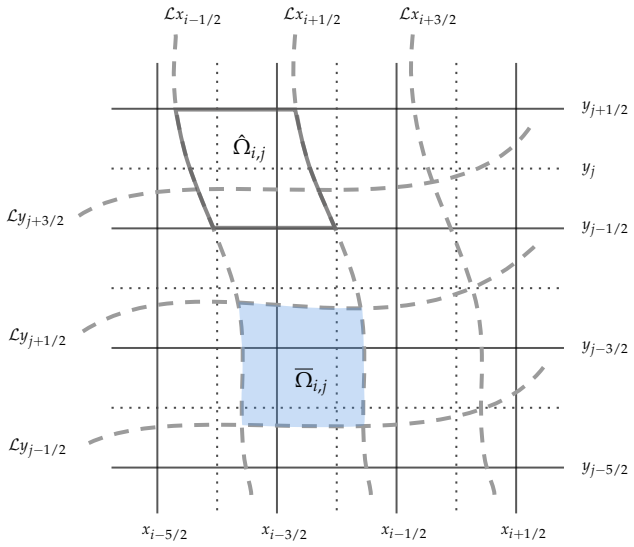

Figure 2: The Eulerian mesh grids (continuous thin black lines), the Eulerian mesh centerlines (dashed thin black lines) and the Lagrangian tracking mesh grids (dashed thick gray lines). $\bar{\Omega}_{i,j}$ is the tracking cell of $\Omega_{i,j}$. $\hat{\Omega}_{i,j}$ is the intermediate cell.

with mass conservation. It is worth noting that the size of the tracking cell $\bar{\Omega}_{i,j}$ remains $h_x h_y$ under the condition of $\nabla\cdot\boldsymbol{u}=0$ [20].

Note that the operator $\mathcal{Q}$ for the diffusion term defined in (3.4) cannot be implemented on the tracking mesh as in the one-dimensional case for that the condition $\nabla\cdot\boldsymbol{u}=0$ only keeps the size of the tracking cell unchanged [20], but not the relative position. Given the misalignment between the tracking mesh and the standard Eulerian mesh, calculating a high-order accuracy approximation of the diffusion term on the irregular tracking mesh with the property of mass conservation while solving the two-dimensional problem (3.1a)-(3.1c) becomes a challenging task.

To approximate the integral of the diffusion term on the tracking cell $\bar{\Omega}_{i,j}$ at time level t^n, we transform it into a line integral along the boundary of the tracking cell, i.e., $\int_{\partial\bar{\Omega}_{i,j}}(K\nabla c(\boldsymbol{x},t^n))\cdot\boldsymbol{n}\mathrm{d}s$ with $\boldsymbol{n}$ being the unit outer normal to the boundary of $\bar{\Omega}_{i,j}$, using Green's formula. We employ a piecewise biquartic function to approximate the scalar field of $c(\boldsymbol{x},t^n)$, which enables us to obtain a high-precision diffusion flux that maintains continuity at the boundary of the tracking cell $\bar{\Omega}_{i,j}$ at time level t^n [12]. Based on the numerical solutions on the uniform Eulerian mesh, we establish the piecewise biquartic polynomial on $\Omega_{i,j}$ as

$$\tilde{\mathcal{C}}^n_{i,j}(x,y)=\sum_{l,m=-2}^{2}\omega_l(\xi)\omega_m(\eta)C^n_{i+l,j+m},\quad i=1,2,\cdots,I;\quad j=1,2,\cdots,J,\tag{3.7}$$

with

$$\xi=(x-x_i)/h_x,\quad \eta=(y-y_j)/h_y, \tag{3.8a}$$

$$\begin{cases} \omega_{-2}(\xi)=(\xi+1)\xi(\xi-1)(\xi-2)/24, \\ \omega_{-1}(\xi)=-(\xi+2)\xi(\xi-1)(\xi-2)/6, \\ \omega_0(\xi)=(\xi+2)(\xi+1)(\xi-1)(\xi-2)/4, \\ \omega_1(\xi)=-(\xi+2)(\xi+1)\xi(\xi-2)/6, \\ \omega_2(\xi)=(\xi+2)(\xi+1)\xi(\xi-1)/24. \end{cases} \tag{3.8b}$$

Utilizing the piecewise function constructed above, the diffusion term approximation at $\bar{\boldsymbol{x}}_{i,j}$ can be solved as

$$\bar{\mathcal{Q}}(C^n)_{\bar{\Omega}_{i,j}}=\frac{1}{h_xh_y}\Big([DI]_{\partial\bar{\Omega}_{i,j,E}}(C^n)+[DI]_{\partial\bar{\Omega}_{i,j,W}}(C^n)+[DI]_{\partial\bar{\Omega}_{i,j,N}}(C^n)+[DI]_{\partial\bar{\Omega}_{i,j,S}}(C^n)\Big), \tag{3.9}$$

where $[DI]_{\partial\bar{\Omega}_{i,j,S}}(C^n)$, $[DI]_{\partial\bar{\Omega}_{i,j,E}}(C^n)$, $[DI]_{\partial\bar{\Omega}_{i,j,N}}(C^n)$ and $[DI]_{\partial\bar{\Omega}_{i,j,W}}(C^n)$ are high accurate approximations for the integral of $(K\nabla c(\boldsymbol{x},t^n))\cdot\boldsymbol{n}$ along "south", "east", "north" and "west" boundaries of $\bar{\Omega}_{i,j}$, respectively.

3.2 Characteristic SSP scheme

Combine the optimal three-stage fourth-order implicit SSP Runge-Kutta method [17] with the characteristic technique to achieve a full-discretization scheme just as in the one-dimensional case. However, solving directly for the values on the irregular tracking mesh with the implicit method is difficult. Noting the definition (2.13), we choose to solve for values on the uniform Eulerian mesh $\Omega_{i,j}$ at $t=t^n+t^{(s)}$ for $s=1,2,3,4$, and apply the conservative interpolation reconstruction technique mentioned above to obtain the values on the tracking cell.

To describe more clearly, we define the space-time domain $\Theta^s_{i,j}$ as

$$\Theta^s_{i,j}=\{(\boldsymbol{x},t)\in\Omega\times[0,T]:\boldsymbol{x}=\boldsymbol{X}(t;t^n+t^{(s)},\boldsymbol{x}^*),\ \boldsymbol{x}^*\in\Omega_{i,j},\ t\in[t^n,t^n+t^{(s)}]\},\quad s=1,2,3,4,$$

And the following are the unified definitions for the tracking cells:

$$\bar{\Omega}^{(k),1}_{i,j}=\{\boldsymbol{x}\in\Omega:\boldsymbol{x}=\boldsymbol{X}(t^n+t^{(k)};t^n+t^{(1)},\boldsymbol{x}^*),\ \boldsymbol{x}^*\in\Omega_{i,j}\},\qquad k=0, \tag{3.10a}$$

$$\bar{\Omega}^{(k),2}_{i,j}=\{\boldsymbol{x}\in\Omega:\boldsymbol{x}=\boldsymbol{X}(t^n+t^{(k)};t^n+t^{(2)},\boldsymbol{x}^*),\ \boldsymbol{x}^*\in\Omega_{i,j}\},\qquad k=0,1, \tag{3.10b}$$

$$\bar{\Omega}^{(k),3}_{i,j}=\{\boldsymbol{x}\in\Omega:\boldsymbol{x}=\boldsymbol{X}(t^n+t^{(k)};t^n+t^{(3)},\boldsymbol{x}^*),\ \boldsymbol{x}^*\in\Omega_{i,j}\},\qquad k=0,1,2, \tag{3.10c}$$

$$\bar{\Omega}^{(k),4}_{i,j}=\{\boldsymbol{x}\in\Omega:\boldsymbol{x}=\boldsymbol{X}(t^n+t^{(k)};t^n+t^{(4)},\boldsymbol{x}^*),\ \boldsymbol{x}^*\in\Omega_{i,j}\},\qquad k=0,1,2,3, \tag{3.10d}$$

which all can be identified by solving problem (3.2) with the fourth-order Runge-Kutta method. That is to say, $\bar{\Omega}^{(k),s}_{i,j}$ represents the tracking cell of $\Omega_{i,j}$ from $t^n+t^{(s)}$ to $t^n+t^{(k)}$ based on $\Theta^s_{i,j}$.

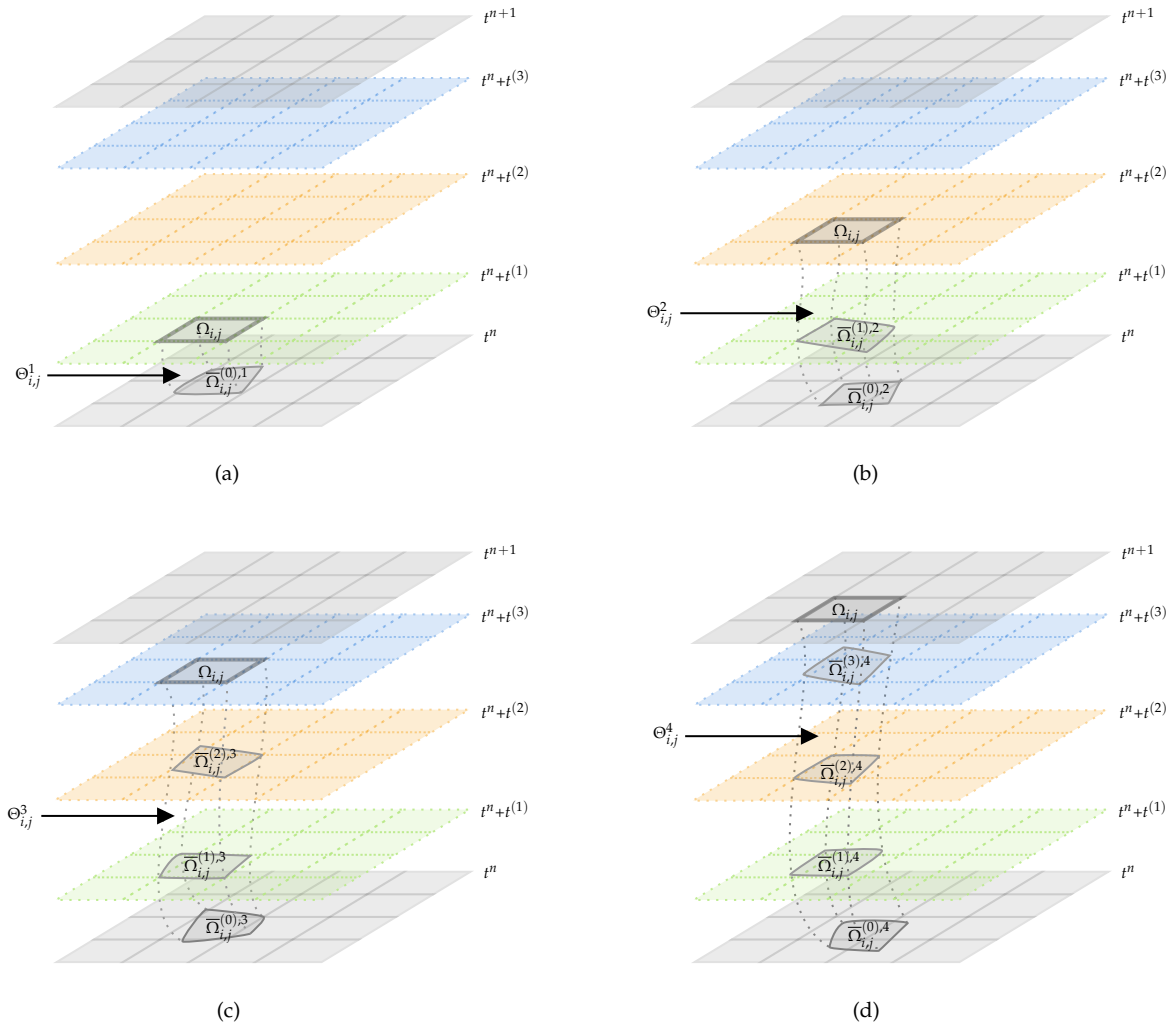

Figure 3: The schematic diagrams for the space-time domains and the corresponding characteristic tracking of $\Omega_{i,j}$.

Figs. 3(a)-(d) present the space-time domains $\Theta_{i,j}^1$, $\Theta_{i,j}^2$, $\Theta_{i,j}^3$ and $\Theta_{i,j}^4$, respectively, and the tracking cells based on the different space-time domains are all marked in the figure.

For the Eulerian cell, let $C_{i,j}^{(k)}$ be the approximation for the average of the solution on $\Omega_{i,j}$ at $t=t^n+t^{(k)}$. Then we denote the approximation for the average of the solution on the irregular cell $\bar{\Omega}_{i,j}^{(k),s}$ by $\bar{C}_{i,j}^{(k),s}$, whose definition can be expressed as

$$\bar{C}_{i,j}^{(k),s}=\frac{1}{h_x h_y}\mathcal{I}_{\bar{\Omega}_{i,j}^{(k),s}}(C^{(k)}). \tag{3.11}$$

Particularly it can be known that $\bar{\Omega}_{i,j}^{(0),4}$ and $\bar{\Omega}_{i,j}$ defined earlier represent the same tracking cell, meanwhile $C_{i,j}^{(4)}$, $C_{i,j}^{(0)}$ and $\bar{C}_{i,j}^{(0),4}$ are actually $C_{i,j}^{n+1}$, $C_{i,j}^{n}$ and $\bar{C}_{i,j}^{n}$, respectively. For solving the two-dimensional convection-diffusion problem (3.1a)-(3.1c), we propose the conservative characteristic spatial-temporal fourth-order method (CC-S4T4-FDM) by modifying the optimal three-stage fourth-order implicit SSP Runge-Kutta method [17], which can be implemented in every time interval $[t^n,t^{n+1}]$ as follows:

Step 1. Calculate the numerical approximation solution $C_{i,j}^{(1)}$ on the Eulerian cell $\Omega_{i,j}$ at $t=t^n+t^{(1)}$ based on the space-time domain $\Theta_{i,j}^{1}$:

$$\bar{C}_{i,j}^{(0),1}=\frac{1}{h_xh_y}\mathcal{I}_{\bar{\Omega}_{i,j}^{(0),1}}(C^{(0)}), \tag{3.12a}$$

$$C_{i,j}^{(1)}=v_1\bar{C}_{i,j}^{(0),1}+\Delta t\beta_{11}\mathcal{Q}(C^{(1)})_{i,j}, \tag{3.12b}$$

Step 2. Calculate the numerical approximation solution $C_{i,j}^{(2)}$ on the Eulerian cell $\Omega_{i,j}$ at $t=t^n+t^{(2)}$ based on the space-time domain $\Theta_{i,j}^{2}$:

$$\bar{C}_{i,j}^{(k),2}=\frac{1}{h_xh_y}\mathcal{I}_{\bar{\Omega}_{i,j}^{(k),2}}(C^{(k)}),\quad k=0,1, \tag{3.13a}$$

$$C_{i,j}^{(2)}=v_2\bar{C}_{i,j}^{(0),2}+\alpha_{21}\bar{C}_{i,j}^{(1),2}+\Delta t\beta_{21}\bar{\mathcal{Q}}(C^{(1)})_{\bar{\Omega}_{i,j}^{(1),2}}+\Delta t\beta_{22}\mathcal{Q}(C^{(2)})_{i,j}, \tag{3.13b}$$

Step 3. Calculate the numerical approximation solution $C_{i,j}^{(3)}$ on the Eulerian cell $\Omega_{i,j}$ at $t=t^n+t^{(3)}$ based on the space-time domain $\Theta_{i,j}^{3}$:

$$\bar{C}_{i,j}^{(k),3}=\frac{1}{h_xh_y}\mathcal{I}_{\bar{\Omega}_{i,j}^{(k),3}}(C^{(k)}),\quad k=0,2, \tag{3.14a}$$

$$C_{i,j}^{(3)}=v_3\bar{C}_{i,j}^{(0),3}+\alpha_{32}\bar{C}_{i,j}^{(2),3}+\Delta t\beta_{32}\bar{\mathcal{Q}}(C^{(2)})_{\bar{\Omega}_{i,j}^{(2),3}}+\Delta t\beta_{33}\mathcal{Q}(C^{(3)})_{i,j}, \tag{3.14b}$$

Step 4. Combine all the above results to calculate $C_{i,j}^{n+1}$ based on the space-time domain $\Theta_{i,j}^{4}$:

$$\bar{C}_{i,j}^{(k),4}=\frac{1}{h_xh_y}\mathcal{I}_{\bar{\Omega}_{i,j}^{(k),4}}(C^{(k)}),\quad k=0,1,2,3, \tag{3.15a}$$

$$\begin{aligned}C_{i,j}^{n+1}=&v_4\bar{C}_{i,j}^{(0),4}+\alpha_{41}\bar{C}_{i,j}^{(1),4}+\alpha_{42}\bar{C}_{i,j}^{(2),4}+\alpha_{43}\bar{C}_{i,j}^{(3),4}+\Delta t\beta_{41}\bar{\mathcal{Q}}(C^{(1)})_{\bar{\Omega}_{i,j}^{(1),4}}\\&+\Delta t\beta_{42}\bar{\mathcal{Q}}(C^{(2)})_{\bar{\Omega}_{i,j}^{(2),4}}+\Delta t\beta_{43}\bar{\mathcal{Q}}(C^{(3)})_{\bar{\Omega}_{i,j}^{(3),4}},\end{aligned} \tag{3.15b}$$

where all the SSP coefficients above are identified as in the one-dimensional case.

3.3 Mass conservation

Hypothesis 3.1. The velocity $\boldsymbol{u}\in C^0(W^{1,\infty}(\Omega))$ satisfies

$$\boldsymbol{u}\cdot\boldsymbol{n}=0 \quad \text{on } \partial\Omega. \tag{3.16}$$

According to Hypothesis 3.1 and the homogeneous Neumann boundary condition (3.1b), it can be set that

$$\hat{H}_{\frac{1}{2},j}(C^{(k)})=\hat{H}_{I+\frac{1}{2},j}(C^{(k)})=\hat{H}_{i,\frac{1}{2}}(C^{(k)})=\hat{H}_{i,J+\frac{1}{2}}(C^{(k)})=0, \quad k=1,2,3,4, \tag{3.17}$$

to implement the numerical scheme (3.12a)-(3.15b).

Theorem 3.1. *Under Hypothesis* 3.1*, the proposed scheme* (3.12a)-(3.15b) *for solving the two-dimensional convection-diffusion problems* (3.1a) *with the homogeneous Neumann boundary condition* (3.1b) *is globally mass conservative.*

Proof. For Step 1, multiplying (3.12b) by h_xh_y and summing for i from 1 to I; j from 1 to J, it follows that

$$\sum_{i=1}^{I}\sum_{j=1}^{J}h_xh_yC_{i,j}^{(1)}=v_1\sum_{i=1}^{I}\sum_{j=1}^{J}h_xh_y\bar{C}_{i,j}^{(0),1}+\Delta t\beta_{11}\sum_{i=1}^{I}\sum_{j=1}^{J}h_xh_y\mathcal{Q}(C^{(1)})_{i,j}. \tag{3.18}$$

Under Hypothesis 3.1, it can be known that there is no flow at the domain boundary. Applying the definition of $\bar{C}_{i,j}^{(0),1}$ and the conservative property of the high-order interpolation [7,12], we have

$$\sum_{i=1}^{I}\sum_{j=1}^{J}h_xh_y\bar{C}_{i,j}^{(0),1}=\sum_{i=1}^{I}\sum_{j=1}^{J}h_xh_yC_{i,j}^{n}. \tag{3.19}$$

According to the boundary condition (3.17) for the numerical scheme and the continuity of $\hat{H}(\cdot)$, it holds that

$$\begin{aligned}
&\sum_{i=1}^{I}\sum_{j=1}^{J}h_xh_y\mathcal{Q}(C^{(1)})_{i,j}\\
=&\sum_{i=1}^{I}\sum_{j=1}^{J}h_xh_y\left(\frac{\hat{H}_{i+\frac{1}{2},j}(C^{(1)})-\hat{H}_{i-\frac{1}{2},j}(C^{(1)})}{h_x}+\frac{\hat{H}_{i,j+\frac{1}{2}}(C^{(1)})-\hat{H}_{i,j-\frac{1}{2}}(C^{(1)})}{h_y}\right)\\
=&\sum_{i=1}^{I}\sum_{j=1}^{J}\Big(h_y(\hat{H}_{i+\frac{1}{2},j}(C^{(1)})-\hat{H}_{i-\frac{1}{2},j}(C^{(1)}))+h_x(\hat{H}_{i,j+\frac{1}{2}}(C^{(1)})-\hat{H}_{i,j-\frac{1}{2}}(C^{(1)}))\Big)\\
=&h_y\sum_{j=1}^{J}(\hat{H}_{I+\frac{1}{2},j}(C^{(1)})-\hat{H}_{\frac{1}{2},j}(C^{(1)}))+h_x\sum_{i=1}^{I}(\hat{H}_{i,J+\frac{1}{2}}(C^{(1)})-\hat{H}_{i,\frac{1}{2}}(C^{(1)}))=0.
\end{aligned} \tag{3.20}$$

Note that $v_1=1$ and combine (3.18)-(3.20), then it yields

$$\sum_{i=1}^{I}\sum_{j=1}^{J}h_xh_yC_{i,j}^{(1)}=\sum_{i=1}^{I}\sum_{j=1}^{J}h_xh_yC_{i,j}^{n}. \tag{3.21}$$

For Step 2, we have that

$$\sum_{i=1}^{I}\sum_{j=1}^{J}h_xh_y\bar{C}_{i,j}^{(0),2}=\sum_{i=1}^{I}\sum_{j=1}^{J}h_xh_yC_{i,j}^{n}, \tag{3.22a}$$

$$\sum_{i=1}^{I}\sum_{j=1}^{J}h_xh_y\bar{C}_{i,j}^{(1),2}=\sum_{i=1}^{I}\sum_{j=1}^{J}h_xh_yC_{i,j}^{(1)}=\sum_{i=1}^{I}\sum_{j=1}^{J}h_xh_yC_{i,j}^{n}, \tag{3.22b}$$

just as the analysis for (3.19). By multiplying (3.13b) with h_xh_y and summing for i ranging from 1 to I, and j from 1 to J, while considering $v_2+\alpha_{21}=1$ and (3.22), it can be deduced that

$$\begin{aligned}\sum_{i=1}^{I}\sum_{j=1}^{J}h_xh_yC_{i,j}^{(2)}=&\sum_{i=1}^{I}\sum_{j=1}^{J}h_xh_yC_{i,j}^{n}+\Delta t\beta_{21}\sum_{i=1}^{I}\sum_{j=1}^{J}h_xh_y\bar{\mathcal{Q}}(C^{(1)})_{\bar{\Omega}_{i,j}^{(1),2}}\\&+\Delta t\beta_{22}\sum_{i=1}^{I}\sum_{j=1}^{J}h_xh_y\mathcal{Q}(C^{(2)})_{i,j}.\end{aligned} \tag{3.23}$$

Under the boundary condition (3.17), we can similarly achieve

$$\sum_{i=1}^{I}\sum_{j=1}^{J}h_xh_y\mathcal{Q}(C^{(2)})_{i,j}=0. \tag{3.24}$$

In fact, it can yield that the entire tracking domain is the same as the Eulerian domain from Hypothesis 3.1. According to the continuity of the discrete fluxes on the boundaries of the tracking cell $\bar{\Omega}_{i,j}^{(1),2}$ and the corresponding proof in [12], we have

$$\sum_{i=1}^{I}\sum_{j=1}^{J}h_xh_y\bar{\mathcal{Q}}(C^{(1)})_{\bar{\Omega}_{i,j}^{(1),2}}=0. \tag{3.25}$$

From (3.23)-(3.25), we obtain that

$$\sum_{i=1}^{I}\sum_{j=1}^{J}h_xh_yC_{i,j}^{(2)}=\sum_{i=1}^{I}\sum_{j=1}^{J}h_xh_yC_{i,j}^{n}. \tag{3.26}$$

Then we handle other steps in a similar way as above. Finally, it leads to

$$\sum_{i=1}^{I}\sum_{j=1}^{J}h_xh_yC_{i,j}^{n+1}=\sum_{i=1}^{I}\sum_{j=1}^{J}h_xh_yC_{i,j}^{n}. \tag{3.27}$$

Thus, we complete the proof. □

4 Numerical experiments

4.1 One-dimensional case

Example 4.1. We now consider a one-dimensional convection-dominated diffusion problem with the periodic boundary condition in $\Omega=[0,2]$, the exact solution of which is given as

$$c(x,t)=1+\exp(-\pi^2 Kt)\sin(\pi x-\pi ut), \tag{4.1}$$

with u and K being the convection velocity and the diffusion coefficient, respectively. The initial condition can be identified from (4.1) by setting $t=0$. We calculate the numerical solution to the final time $T=1$ with $K=10^{-5}$ and different $u=1$ and 10.

To demonstrate the superiority of our proposed conservative characteristic spatial-temporal fourth-order finite difference method (CC-S4T4-FDM), a scheme that use SSP Runge-Kutta method directly and does not employ the characteristics technique (C-S4T4-FDM) is introduced for comparison. The sole distinction between this non-characteristic C-S4T4-FDM and the proposed CC-S4T4-FDM lies in the treatment of the convection term. Specifically, the non-characteristic scheme is processed with the following central fourth-order difference operator

$$\mathcal{P}^*(C)_i=\frac{C_{i-2}-8C_{i-1}+8C_{i+1}-C_{i+2}}{12h}$$

to handle the first-order derivative of the convection term.

We now check the spatial and temporal convergence orders of the numerical solutions calculated by the CC-S4T4-FDM and the aforementioned non-characteristic C-S4T4-FDM. Choosing different step sizes of $\Delta t=h=\frac{1}{30}$, $\frac{1}{40}$, $\frac{1}{50}$ and $\frac{1}{60}$ to compute errors measured by the discrete L^2- norm and L^∞- norm, the results for the convection velocity $u=1$ and 10 are illustrated in Table 1 and Table 2, respectively. It is clearly shown in Table 1

Table 1: Errors, convergence ratios and mass errors of the numerical solutions of the CC-S4T4-FDM and the non-characteristic C-S4T4-FDM with $u=1$.

	I	60	80	100	120
CC-S4T4-FDM	L^∞- error	1.3157e-10	4.1675e-11	1.7111e-11	8.2368e-12
	Ratio	-	3.9962	3.9893	4.0099
	L^2- error	1.3174e-10	4.1706e-11	1.7101e-11	8.2332e-12
	Ratio	-	3.9982	3.9952	4.0093
	mass error	1.9895e-14	4.2633e-15	3.4674e-14	1.8237e-14
C-S4T4-FDM	L^∞- error	1.2286e-05	3.8919e-06	1.5950e-06	7.6939e-07
	Ratio	-	3.9960	3.9976	3.9984
	L^2- error	1.2302e-05	3.8948e-06	1.5957e-06	7.6965e-07
	Ratio	-	3.9980	3.9988	3.9992
	mass error	8.5265e-15	2.8422e-15	2.2737e-15	3.7896e-15

Table 2: Errors, convergence ratios and mass errors of the numerical solutions of the CC-S4T4-FDM and the non-characteristic C-S4T4-FDM with $u=10$.

	I	60	80	100	120
CC-S4T4-FDM	L^∞- error	1.3169e-10	4.1861e-11	1.7138e-11	8.3691e-12
	Ratio	-	3.9837	4.0022	3.9313
	L^2- error	1.3174e-10	4.1703e-11	1.7100e-11	8.2336e-12
	Ratio	-	3.9984	3.9953	4.0085
	mass error	1.5395e-14	6.7502e-15	3.2401e-14	1.2316e-14
C-S4T4-FDM	L^∞- error	3.0668e+13	1.0379e+23	3.0681e+32	2.6825e+42
	Ratio	-	-7.6273e+01	-9.7727e+01	-1.2556e+02
	L^2- error	2.3408e+13	6.7130e+22	1.9398e+32	1.6139e+42
	Ratio	-	-7.5698e+01	-9.7625e+01	-1.2528e+02
	mass error	3.9063e-04	2.0972e+06	5.7646e+15	3.6107e+25

that our proposed CC-S4T4-FDM and the non-characteristic C-S4T4-FDM attain fourth-order accuracy in both time and space with $u=1$, and conserve mass effectively. The L^∞- errors and L^2- errors of the CC-S4T4-FDM are noticeably smaller than those of the non-characteristic C-S4T4-FDM under the identical parameter conditions. That is to say, our proposed CC-S4T4-FDM can yield satisfactory high-precision numerical results with relatively larger discretization step sizes.

Table 2 shows the results under the condition of large convection velocity of $u=10$. It can be seen that the CC-S4T4-FDM still maintains spatial-temporal fourth-order accuracy and mass conservation while the numerical solution obtained using the non-characteristic C-S4T4-FDM exhibits severe oscillations and can not get correct results. Choosing the time steps of $N_t=30$ and the space steps of $I=30$, we perform computations using both the CC-S4T4-FDM and the non-characteristic C-S4T4-FDM to solve (4.1) with $K=10^{-5}$ and $u=10$. The numerical solutions at time $t=1$ are presented in Fig. 4, alongside the exact solution. Comparing to non-characteristic C-S4T4-FDM, it is evident that our proposed CC-S4T4-FDM allows for the use of fairly larger time step sizes in computations without inducing numerical oscillations, which can significantly reduce computational costs.

4.2 Two-dimensional case

Example 4.2. In this example, we study the two-dimensional convection-diffusion problem by considering the rotating Gaussian concentration pulse in the spatial domain $\Omega=[-1,1]\times[-1,1]$ with the variable velocity field of $(u^x,u^y)=(-\lambda y,\lambda x)$, where the different values of λ determine different velocity fields. The analytical solution to the problem is given as

$$c(x,y,t)=\frac{\sigma_0^2}{\sigma_0^2+2Kt}\exp\left(-\frac{(\overline{x}(t)-x_0)^2+(\overline{y}(t)-y_0)^2}{2\sigma_0^2+4Kt}\right), \tag{4.2}$$

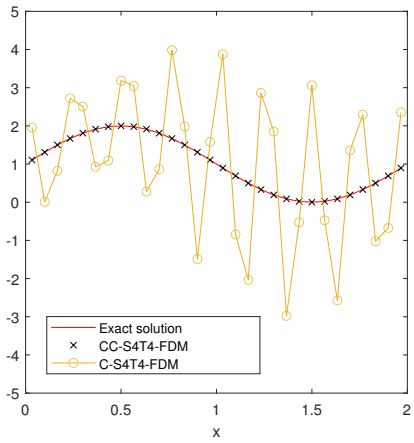

Figure 4: Comparison of the different numerical solutions for Example 4.1 by the propose CC-S4T4-FDM and Non-Characteristic C-S4T4-FDM at time $t=1$ with $K=10^{-5}$ and $u=10$.

where $(x_0,y_0)=(-0.35,0)$ represents the initial center of the Gaussian pulse, $\sigma_0=0.07$ denotes the standard deviation, $\overline{x}(t)$ and $\overline{y}(t)$ are defined as

$$\overline{x}(t)=x\cos(\lambda t)+y\sin(\lambda t),\quad \overline{y}(t)=-x\sin(\lambda t)+y\cos(\lambda t).$$

The initial condition is given by setting $t=0$ in the analytical solution (4.2) and the boundary condition is considered as the homogeneous Neumann boundary condition. Then we calculate to the final time $T=1/5$ with the diffusion coefficient of $K^x=K^y=K=10^{-5}$ to examine the convergence rates and mass conservation property of the proposed numerical scheme.

In Table 3 and Table 4, we examine the convergence ratios of the proposed CC-S4T4-FDM for two-dimensional convection-diffusion problems with different velocity fields, respectively. Choose different step sizes of $\Delta t=h_x=h_y=\frac{1}{30}$, $\frac{1}{40}$, $\frac{1}{50}$ and $\frac{1}{60}$ to execute the scheme and calculate errors using the discrete L^2- norm and L^∞- norm, where the fourth-order Runge-Kutta method is applied to identify the tracking points during the characteristics tracking process. It is clear that the proposed scheme has spatial and temporal fourth-order accuracy. The mass conservative property can also be verified according to Table 3 and Table 4, which corroborate the theoretical results.

Table 3: Errors, convergence ratios and mass errors of the numerical solutions of the CC-S4T4-FDM with $\lambda=4$.

I	60	80	100	120
L^∞- error	1.3661e-02	4.5977e-03	1.8559e-03	8.5329e-04
Ratio	-	3.7854	4.0654	4.2619
L^2- error	1.1445e-03	3.7414e-04	1.5263e-04	7.2677e-05
Ratio	-	3.8865	4.0181	4.0698
mass error	2.6923e-15	5.8981e-17	1.0408e-17	6.9389e-18

Table 4: Errors, convergence ratios and mass errors of the numerical solutions of the CC-S4T4-FDM with $\lambda=20$.

I	60	80	100	120
L^∞- error	1.6939e-02	5.4727e-03	2.1024e-03	9.1482e-04
Ratio	-	3.9275	4.2873	4.5640
L^2- error	1.5851e-03	4.9152e-04	2.0152e-04	9.6376e-05
Ratio	-	4.0700	3.9957	4.0458
mass error	5.9570e-15	1.5959e-16	6.9389e-18	1.0408e-17

Example 4.3. Consider the convection-diffusion problem for a convected wave over a two-dimensional spatial domain $\Omega=[-\pi,\pi]\times[-\pi,\pi]$. The divergence free velocity field is

$$\vec{u}=(u^x,u^y)=\left(\frac{\partial\psi}{\partial y},-\frac{\partial\psi}{\partial x}\right)$$

with $\psi(x,y)$ being defined as

$$\psi(x,y)=\frac{1}{4}\sin^2(x)\cos^2\left(y-\frac{\pi}{2}\right)-\frac{\pi y}{20}. \tag{4.3}$$

The initial condition $c(x,y,0)$ is given by

$$\begin{aligned}c(x,y,0)=&\frac{1}{4}\left\{\text{erf}\left(\frac{x_1-x+10^{-2}}{0.3}\right)+\text{erf}\left(\frac{-x_0+x-10^{-2}}{0.3}\right)\right\}\\&\times\left\{\text{erf}\left(\frac{y_1-y+10^{-2}}{0.3}\right)+\text{erf}\left(\frac{-y_0+y-10^{-2}}{0.3}\right)\right\},\end{aligned} \tag{4.4}$$

where $x_0=\frac{\pi}{5}$, $x_1=\frac{3\pi}{5}$, $y_0=-\frac{\pi}{3}$, $y_1=\frac{2\pi}{3}$ and $\text{erf}(x)=\frac{2}{\sqrt{\pi}}\int_0^x\exp(-\eta^2)\text{d}\eta$ is the error function. The velocity field and the initial value distribution are shown in Fig. 5. Consider the

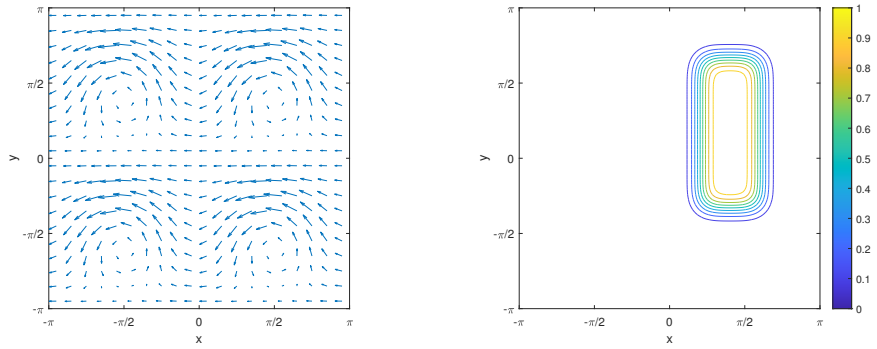

(a) (b)

Figure 5: (a) The velocity field of $\boldsymbol{u}=(u^x,u^y)=\left(\frac{\partial\psi}{\partial y},-\frac{\partial\psi}{\partial x}\right)$. (b) Initial value distribution.

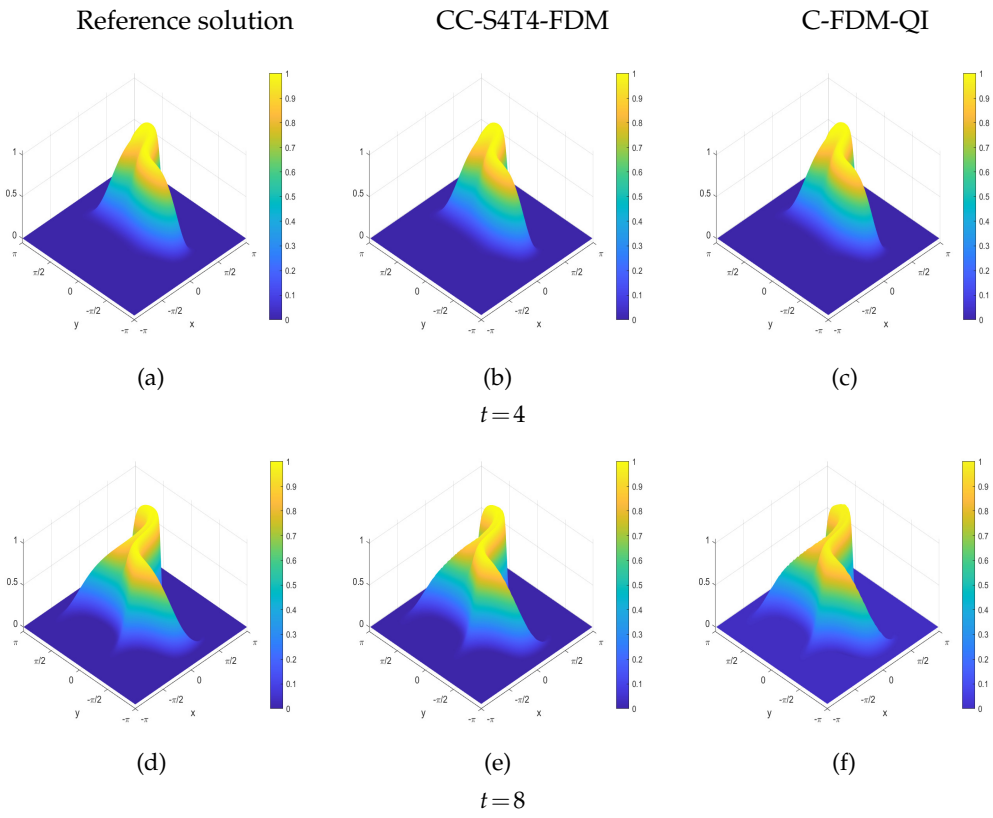

Figure 6: The three-dimensional view of the moving wave.

diffusion coefficient to be $K^x=K^y=10^{-5}$ and evaluate the reference exact solution at the final time $T=8$ with the CC-S4T4-FDM using fine mesh of $I=J=500$ and $N_t=90$. Then the constructed CC-S4T4-FDM and the characteristic finite difference method with bi-quadratic interpolation (C-FDM-QI) [11] are performed respectively to attain numerical solutions with $I=J=120$ and $N_t=30$.

Figs. 6, 7 and 8 present the three-dimensional view, x-z view and y-z view respectively of the reference exact solution and the numerical solutions calculated by the CC-S4T4-FDM and the C-FDM-QI at $t=4$ and 8, where we set the same z-axis range $[-0.05,1.05]$ of drawings to maintain the consistency of the graph. According to the comparison in Figs. 6-8, we can know that the numerical solutions calculated by the CC-S4T4-FDM with coarse mesh track the steep front very well and get results almost as same as the reference exact solution, while the numerical solutions of the C-FDM-QI appear noticeable oscillations at $t=8$ as in Fig. 7(f) and Fig. 8(f).

In addition, the above problem is solved by the CC-S4T4-FDM and the C-FDM-QI to the final time $t=30$ in a large domain $\Omega=[-3\pi,3\pi]\times[-3\pi,3\pi]$ with $I=J=360$ and $N_t=60$. The mass percentage and the mass errors of solutions calculated by the CC-S4T4-

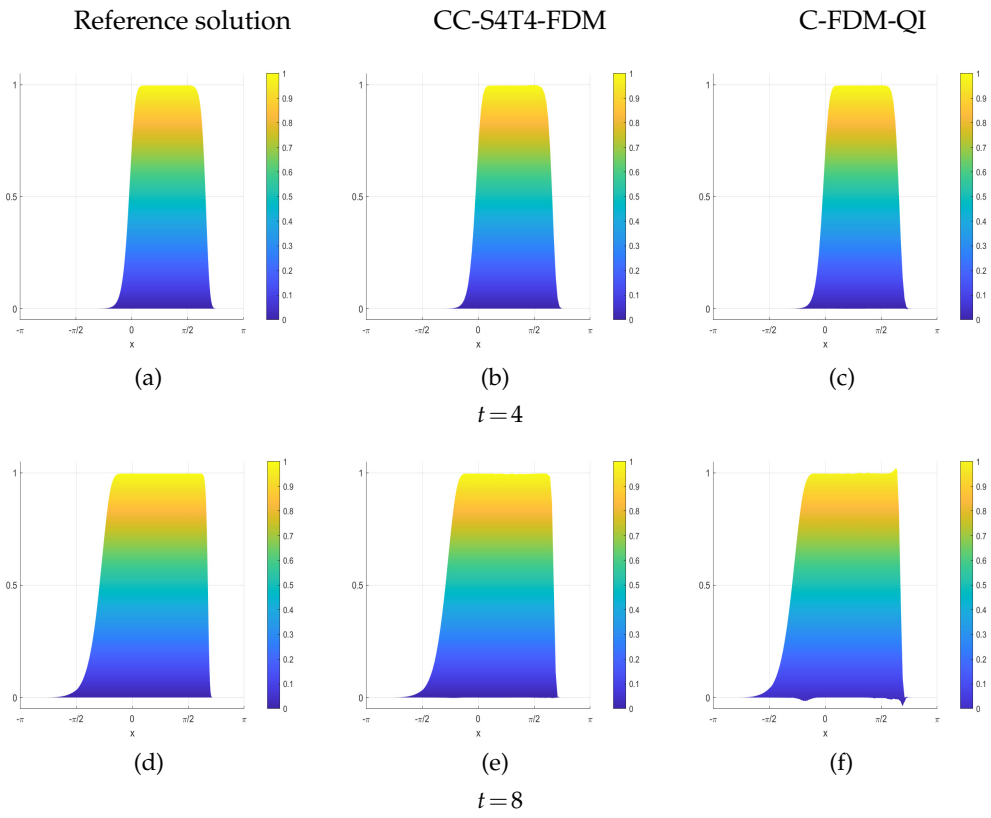

Figure 7: The x-z view of the moving wave.

FDM and the C-FDM-QI are shown in Fig. 9, which indicates that the CC-S4T4-FDM preserves mass perfectly, while the mass errors for the C-FDM-QI increase significantly as time goes by.

5 Conclusions

We have developed in this paper the conservative characteristic finite difference schemes for convection-dominated diffusion equations that achieve fourth-order accuracy in both space and time. By utilizing the characteristics method, our schemes can effectively employ larger time step sizes. We introduce the modified optimal SSP Runge–Kutta method, coupled with the characteristics technique, to achieve temporal high-order accuracy. To handle the diffusion term, diverse fourth-order approximation operators based on the uniform Eulerian mesh and irregular Lagrangian mesh respectively are constructed. Our approach is theoretically proven to be mass conservative, making it appropriate for large scale scientific simulations and areas where mass conservation is of paramount impor-

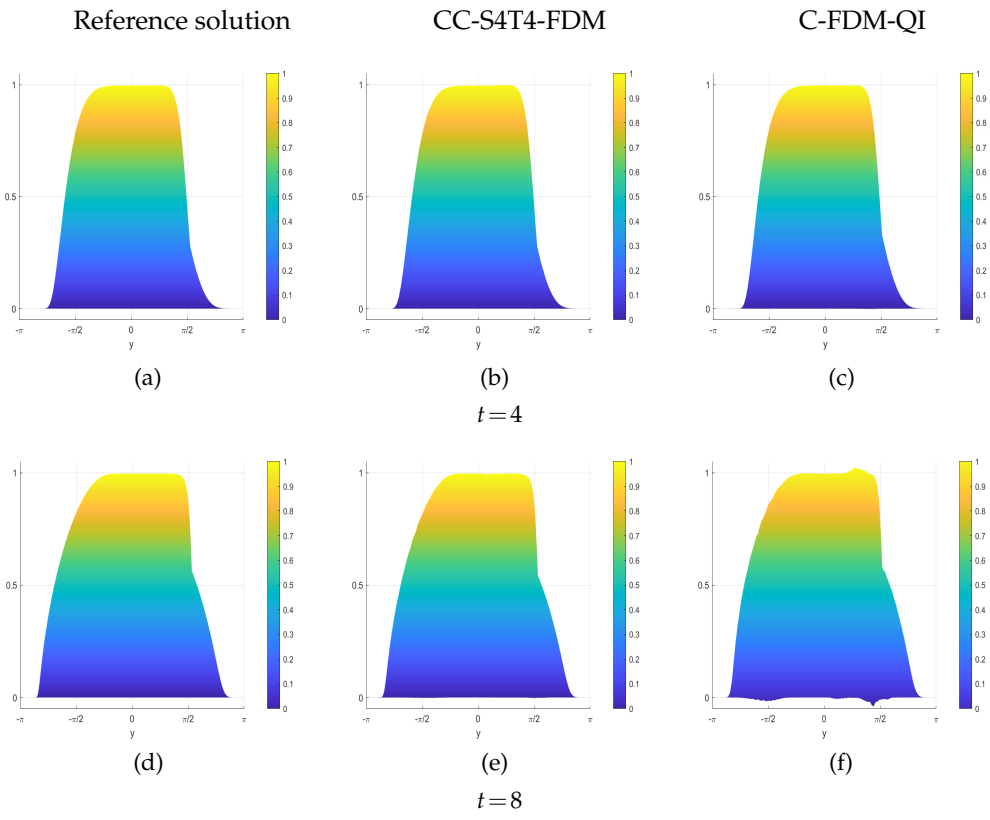

Figure 8: The y-z view of the moving wave.

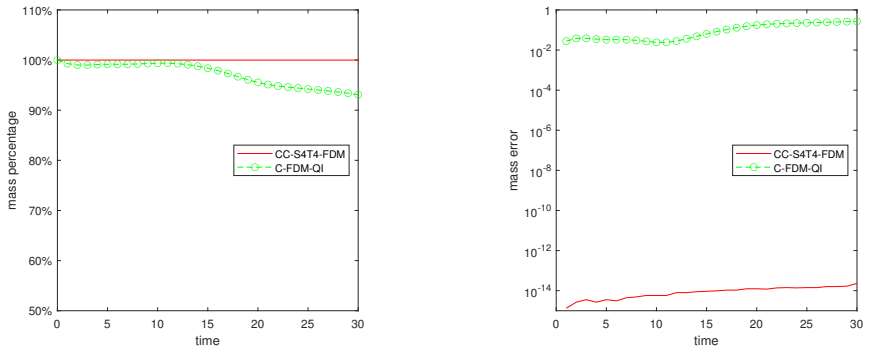

Figure 9: (a) Time series of the mass percentage. (b) Time series of the mass errors.

tance. The temporal and spatial convergence orders of the proposed scheme are practically verified by numerical experiments. Moreover, we observe that our numerical

method conserves mass and effectively avoids numerical oscillations even when using large time step sizes. Overall, our work presents a robust and accurate numerical method for efficiently solving convection-dominated diffusion equations with mass conservation property.

Acknowledgements

This work was supported partially by National Natural Science Foundation of China (Grant No. 12371412), Fundamental Research Funds for Central Universities of China, Natural Science Foundation of Shandong Province (Grant No. ZR2021MA005), Natural Sciences and Engineering Research Council of Canada, and Qingdao Natural Science Foundation (23-2-1-158-zyyd-jch). We would thank the referees for their valuable suggestions which have helped to improve the paper greatly.

References

[1] T. Arbogast and Mary F. Wheeler, *A characteristics-mixed finite element method for advection-dominated transport problems,* SIAM J. Numer. Anal., 32(2) (1995), pp. 404–424.
[2] Uri M. Ascher, Steven J. Ruuth, and Brian T. R. Wetton, *Implicit-explicit methods for time-dependent partial differential equations,* SIAM J. Numer. Anal., 32(3) (1995), pp. 797–823.
[3] J. Bear, Hydraulics of Groundwater, Dover Books on Engineering, Dover Publications, New York, 1979.
[4] R. Bermejo, *A Galerkin-characteristic algorithm for transport-diffusion equations,* SIAM J. Numer. Anal., 32(2) (1995), pp. 425–454.
[5] E. Celledoni and B. K. Kometa, *Semi-Lagrangian Runge-Kutta exponential integrators for convection dominated problems,* J. Sci. Comput., 41(1) (2009), pp. 139–164.
[6] J. Cheng and C-W.Shu, *Positivity-preserving Lagrangian scheme for multi-material compressible flow,* J. Comput. Phys., 257 (2014), pp. 143–168.
[7] P. Colella and Paul R. Woodward, *The piecewise parabolic method (PPM) for gas-dynamical simulations,* J. Comput. Phys., 54(1) (1984), pp. 174–201.
[8] C. N. Dawson, T. F. Russell, and M. F. Wheeler, *Some improved error estimates for the modified method of characteristics,* SIAM J. Numer. Anal., 26(6) (1989), pp. 1487–1512.
[9] J. Douglas, Jr. and Thomas F. Russell, *Numerical methods for convection-dominated diffusion problems based on combining the method of characteristics with finite element or finite difference procedures,* SIAM J. Numer. Anal., 19(5) (1982), pp. 871–885.
[10] K. Fu and D. Liang, *The conservative characteristic FD methods for atmospheric aerosol transport problems,* J. Comput. Phys., 305 (2016), pp. 494–520.
[11] K. Fu and D. Liang, *The time second order mass conservative characteristic FDM for advection–diffusion equations in high dimensions,* J. Sci. Comput., 73(1) (2017), pp. 26–49.
[12] K. Fu and D. Liang, *A mass-conservative temporal second order and spatial fourth order characteristic finite volume method for atmospheric pollution advection diffusion problems,* SIAM J. Sci. Comput., 41(6) (2019), pp. B1178–B1210.

[13] F. GAO AND Y. YUAN, *The upwind finite volume element method based on straight triangular prism partition for nonlinear convection-diffusion problem,* Appl. Math. Comput., 181(2) (2006), pp. 1229–1242.
[14] F. GAO AND Y. YUAN, *The characteristic finite volume element method for the nonlinear convection-dominated diffusion problem,* Comput. Math. Appl., 56(1) (2008), pp. 71–81.
[15] Y. GAO, Y. LI, G. YUAN, AND Z. SHENG, *New finite volume element methods in the ALE framework for time-dependent convection–diffusion problems in moving domains,* J. Comput. Appl. Math., 393 (2021), 113537.
[16] Y. GAO, D. LIANG, AND Y. LI, *Optimal weighted upwind finite volume method for convection–diffusion equations in 2D,* J. Comput. Appl. Math., 359 (2019), pp. 73–87.
[17] S. GOTTLIEB, D. I. KETCHESON, AND C. W. SHU, Strong Stability Preserving Runge-Kutta and Multistep Time Discretizations, World Scientific, Singapore, 2011.
[18] P. HANSBO, *The characteristic streamline diffusion method for convection-diffusion problems,* Comput. Methods Appl. Mech. Eng., 96(2) (1992), pp. 239–253.
[19] M. HE, P. SUN, C. WANG, AND Z. HUANG, *A two-grid combined finite element-upwind finite volume method for a nonlinear convection-dominated diffusion reaction equation,* J. Comput. Appl. Math., 288 (2015), pp. 223–232.
[20] J. HUA AND J. LOU, *Numerical simulation of bubble rising in viscous liquid,* J. Comput. Phys., 222(2) (2007), pp. 769–795.
[21] R. KAMAKOTI AND C. PANTANO, *High-order narrow stencil finite-difference approximations of second-order derivatives involving variable coefficients,* SIAM J. Sci. Comput., 31(6) (2010), pp. 4222–4243.
[22] H. LENG AND Y. CHEN, *Adaptive hybridizable discontinuous Galerkin methods for nonstationary convection diffusion problems,* Adv. Comput. Math., 46(4) (2020), 50.
[23] A. LI, J. HUANG, W. LIU, H. WEI, AND N. YI, *A characteristic block-centered finite difference method for Darcy–Forchheimer compressible miscible displacement problem,* J. Comput. Appl. Math., 413 (2022), 114303.
[24] X. LI AND K. FU, *Positive and conservative characteristic block-centered finite difference methods for convection dominated diffusion equations,* Adv. Appl. Math. Mech., 14(5) (2022), pp. 1087–1110.
[25] D. LIANG, *A characteristics mixed finite element method of numerical simulation for 2-phase immiscible flow,* Sci. China Ser. A, 9 (1991), pp. 1281–1289.
[26] D. LIANG, K. FU, AND W. WANG, *Modelling multi-component aerosol transport problems by the efficient splitting characteristic method,* Atmospheric Environment, 144 (2016), pp. 297–314.
[27] W. LIU, Y. CHEN, Z. WANG, AND J. HUANG, *Second-order numerical method for coupling of slightly compressible Brinkman flow with advection-diffusion system in fractured media,* J. Comput. Phys., 486 (2023), 112120.
[28] K. W. MORTON, Numerical Solution of Convection-Diffusion Problems, CRC Press, Boca Raton, 1996.
[29] H. RUI AND M. TABATA, *A mass-conservative characteristic finite element scheme for convection-diffusion problems,* J. Sci. Comput., 43(3) (2010), pp. 416–432.
[30] D. SÁRMÁNY, M. A. BOTCHEV, AND J. J. W. VAN DER VEGT, *Dispersion and dissipation error in high-order Runge-Kutta discontinuous Galerkin discretisations of the Maxwell equations,* J. Sci. Comput., 33(1) (2007), pp. 47–74.
[31] S. SENGUPTA, N. A. SREEJITH, P. MOHANAMURALY, G. STAFFELBACH, AND L. GICQUEL, *Global spectral analysis of the Lax–Wendroff-central difference scheme applied to convection–diffusion equation,* Comput. Fluids, 242 (2022), 105508.

[32] JAN C. THIELE, I. GREGOR, N. KAREDLA, AND J. ENDERLEIN, *Efficient modeling of three-dimensional convection–diffusion problems in stationary flows,* Phys. Fluids, 32(11) (2020), 112015.

[33] HENRY TUFO, Improved Transport Processes for CCSM, Technical Report, University of Colorado, 2011.

[34] C. WANG, M. HE, AND P. SUN, *A new combined finite element-upwind finite volume method for convection-dominated diffusion problems,* Numer. Methods Partial Differential Equations, 32(3) (2016), pp. 799–818.

[35] J. WANG, Z. SI, AND W. SUN, *A new error analysis of characteristics-mixed FEMs for miscible displacement in porous media,* SIAM J. Numer. Anal., 52(6) (2014), pp. 3000–3020.

[36] Y. XU AND C-W. SHU, *Error estimates of the semi-discrete local discontinuous Galerkin method for nonlinear convection–diffusion and KdV equations,* Comput. Methods Appl. Mech. Eng., 196(37) (2007), pp. 3805–3822.

[37] Z. ZHANG, Y. WANG, AND Q. WANG, *A characteristic centred finite difference method for a 2D air pollution model,* Int. J. Comput. Math., 88(10) (2011), pp. 2178–2198.

[38] L. ZHOU AND Y. XU, *Stability analysis and error estimates of semi-implicit spectral deferred correction coupled with local discontinuous Galerkin method for linear convection–diffusion equations,* J. Sci. Comput., 77(2) (2018), pp. 1001–1029.

[39] Z. ZHOU, T. HANG, T. JIANG, Q. ZHANG, H. TANG, AND X. CHEN, *Mass conservative characteristic finite difference method for convection–diffusion equations,* Int. J. Comput. Math., 98(10) (2021), pp. 2115–2136.